Experimental and numerical investigations on the effect of porosity and PPI gradients of metal foams on the thermal performance of a composite phase change material heat sink

Girish Kumar Marri, C. Balaji*

Heat Transfer and Thermal Power Laboratory, Department of Mechanical Engineering, Indian Institute of Technology Madras, Chennai 600036, India

ABSTRACT

This paper reports the results of an experimental and numerical study on the thermal performance of a metal foam based composite phase change material (PCM) heat sink cylindrical in shape with porosity and PPI (pores per inch) density gradients. Studies are conducted on different configurations of composite PCM made of an open-cell aluminum metal foams with porosities of 0.9, 0.94 and 0.97 and PPI of 8, 14 and 20 encapsulated with n-eicosane as the PCM. Experiments are carried out on the PCM heat sink heated from the bottom for different configurations of metal foams with a uniform porosity and non-uniform porosity created with layer wise arrangement of metal foams from the bottom to the top. Complementary three-dimensional numerical simulations have been conducted using the enthalpy porosity methodology with a non-thermal equilibrium model to understand the melting and solidification dynamics of PCM while melting (charging) and solidification (discharging) respectively. Heat sink configurations with uniform porosity, and porosity gradient created with bi-layer arrangement of metal foams have been simulated numerically. Further, the numerical simulations have been extended to study heat sink configurations containing metal foams with uniform PPI density and PPI density gradient. From the results, it is seen that the case of non-uniform variation in porosity (decreasing from the bottom to the top) with constant PPI density and the case of non-uniform PPI density (increasing from the bottom to the top) with constant porosity show superior performance up to 28 and 45% over the heat sink configurations with uniform porosity and PPI density respectively in the charging cycle in terms of the time to reach a setpoint temperature. From the numerical simulations, it is seen that the melt fraction of PCM significantly changes the convection velocity cells, which affects the melting dynamics of PCM. Additional numerical simulations have been conducted on PCM heat sink with non-uniform porosity (i.e. decreasing porosity from the bottom to the top) and non-uniform PPI density (i.e increasing PPI density from the bottom to the top) gradients created with three layers (tri-layer) of metal foams. The results show that the PCM heat sink with non-uniform porosity and non-uniform PPI density gradients created with tri-layer metal foams have almost the same performance as a bi-layer metal foam with enhancement ratio up to 4 and 4.4 times respectively over the base line case (i.e. PCM heat sink without metal foams). In the discharging cycle, it is seen that the porosity and PPI gradients do not have any effect on the thermal performance of the heat sink.

© 2020 Elsevier Ltd. All rights reserved.

1. Introduction

Phase change materials (PCMs) have become a promising option in passive thermal management of electronic devices. The incorporation of a phase change material in a heat sink helps control the device temperature for longer periods of time due to high latent heat of PCM [1]. Despite high latent heat, PCMs suffer from a low thermal conductivity (~0.2 W/m.K). Hence, researchers have been exploring the use of thermal conductivity enhancers (TCE) such as the use of fins, mixing of nano particles with the PCM, honey comb inserts and metal foams to enhance the heat diffusion into the PCM for effective exploitation of the latent heat of the PCM [2–5]. Metal foams as a TCE have continuous high conductivity metal paths and voids to encapsulate the PCM in them. Hence, the use of metal foams as TCE helps maintain high metal to PCM contact area

* Corresponding author.
  E-mail address: balaji@iitm.ac.in (C. Balaji).

Nomenclature

a	interfacial surface area, $(1/m)$
C	inertial coefficient, $(1/m)$
c_p	specific heat at constant pressure, $(kJ/kg.K)$
d	diameter, (mm)
g	gravitational acceleration, (m/s^2)
h	interfacial heat transfer coefficient, (W/m^2K)
I	current, (A)
K	permeability, (m^2)
k	thermal conductivity, $(W/m.K)$
l	latent heat capacity, (kJ/kg)
P	power, (W)
Pr	Prandtl Number
p	pressure, (N/m^2)
Re	Reynolds Number
T	temperature, (^oC)
t	time, (s)
U	velocity vector, (m/s)
u, v, w	velocities in the x,y and z directions, (m/s)
V	voltage, (V)
Z	mushy zone constant
α	thermal expansion coefficient, $(1/K)$
β	liquid fraction
χ	tortuosity coefficient
δ	constant
ε	bulk porosity
ϕ	enhancement ratio
μ	dynamic viscosity, $(kg/m\,s)$
ρ	density, (kg/m^3)
σ	uncertainty
eff	effective
f	fiber
k	characteristic length
l	liquidus
mf	metal foam
p	pore
s	solidus

for effective heat transfer to the PCM. Qu et al. [6], experimentally, studied the performance of a hybrid heat sink with metal foam PCM composite and top surface fins. From this study, the authors concluded that either a metal foam with low porosity or a metal foam with high pore density lowers the heater temperature. Lafdi et al. [7] carried out experimental investigations on a composite PCM metal foam with different porosities and pore sizes. They observed faster melting rates of PCM in low porosity and high pores per inch (PPI) metal foams due to faster conduction of heat through metal foams. Chen et al. [8], experimentally and numerically, investigated the melting of PCM in a metal foam at a pore scale level. From their investigations, they concluded that (i) the conduction of heat in a metal foam plays an important role in the melting of the PCM and (ii) metal foam enhances the conduction in PCM by resisting the flow of liquid PCM. Atal et al. [9], experimentally and numerically, studied the effect of porosity of metal foam with PCM on the shell side in a shell and tube heat exchanger, and concluded that the enthalpy porosity methodology shows good agreement with the experimental results. The metal foam with lower porosity showed faster melting rate due to high effective thermal conductivity. Xiao et al. [10] measured and theoretically calculated the effective thermal conductivity of composite PCM and metal foams for different porosity metal foams. The authors concluded that the thermal conductivity of a composite metal foam PCM is significantly enhanced over the pure PCM.

Zheng et al. [11] performed experimental studies on the melting of PCM in a metal foam under three heating modes namely the top, the side and the bottom. They observed that the melting of PCM under top heating mode is slower and the temperature of heater was also found to rise very quickly compared to the other two modes. This implies that the natural convection of liquid PCM in the metal foam plays a significant role in the melting of PCM, and hence cannot be neglected. Tian and Zhao [12] carried out numerical investigations on a PCM encapsulated with metal foam with different porosities and PPI. The authors observed that, metal foams resist the flow of PCM and suppress the convection. This implies that the enhancement of heat transfer caused is due to domination of heat conduction over natural convection in the PCM. The authors also argued that the heat transfer can be enhanced much with lower porosity and higher pore density metal foams. Li et al. [13], experimentally and numerically, investigated the melting of paraffin in an open cell metal foam. The numerical model was validated with experimental results by considering the non Darcy effect, local natural convection and thermal non- equilibrium into the model. The numerical model showed good agreement with the experimental results. The authors also explained the importance of two equation model where two energy equations are simultaneously solved for the heat transfer in PCM and metal foam to simulate the melting of PCM in a metal foam. Cui [14], experimentally, investigated the charging process of paraffin in a high porosity metal foam and showed that the presence of metal foam leads to more uniform temperatures in system, which, in turn significantly enhances the charging rate of energy storage system. Sundarram and Li [15], numerically, investigated the effect of pore size and porosity on PCM filled micro-cellular metal foams. From the results, the authors concluded that, the porosity and pore size have a significant effect on the melting rate of the PCM. For a fixed porosity and lower pore diameter, the results showed a lower heat source temperature for a longer period of time. Feng et al. [16] carried out experimental investigations on freezing rates of a PCM in a metal foam. The authors considered different contact conditions of metal foam with base material such as natural contact, pressurized contact and adhesive bonding. From the results, the authors concluded that the freezing rates of the PCM are independent of the type of contact between the metal foam and the base material. Tao et al. [17] simulated the melting of PCM in a metal foam using the Lattice Boltzmann method. The authors studied the effect of different parameters such as metal foam porosity and pore density on the melting rate of the PCM. The authors also additionally proposed an enhancement technique with the use of a nonuniform porosity metal foam. The proposed technique was found to significantly improve the uniformity in temperature and enhance the heat transfer performance. Zhu et al. [18] developed a finite volume based numerical method with a non-equilibrium equation to study the melting process of PCM in a metal foam in rectangular geometry. The authors also proposed three enhancement techniques namely (i) varying the PPI of metal foam (ii) changing the position of the cold wall and (iii) using discrete heating. Additionally, the authors carried out an optimization study by combining all the proposed enhancement techniques and the optimum configuration was found to have 83.32% faster melting rate over the pure paraffin case. Zhang et al. [19], numerically, investigated the melting of PCM in a metal foam with varying porosity from the top to the bottom and the bottom to the top. The porosity gradient was created by two methods (i) by considering different porosity metal foam slices and (ii) by linearly varying the porosity along the height. From the results, the authors concluded that the porosity gradient enhances the heat transfer rate and that heat conduction dominates the entire heat transfer process. Zhu et al. [20], experimentally, investigated a composite metal foam PCM heat sink at different filling heights of the metal foam. The authors found out

that the optimum filling height of metal foam is 2/3 rd of height of the heat sink, beyond which there was no change in the thermal performance of the heat sink. Joshi and Rathod [21], numerically, investigated the augmentation of thermal transport in a composite metal foam latent thermal energy storage system and proposed a novel configuration of metal foam arrangement to improve the thermal performance of system. From the results, it was seen that providing the metal foam only in the thermal potential regions enhances the thermal performance with conduction heat transfer and results in the same melting time of as that if the case of a PCM completely encapsulated inside a metal foam. Manchin et al. [22], experimentally, investigated the melting of PCM in a copper metal foam for different PPI densities. They concluded that a metal foam improves the melting rates of the PCM and the variation in PPI density did not significantly affect the melting rate of PCM. Yao and Wu [23] performed numerical investigations on the melting process of PCM in high porosity metal foams in pore scale level. They concluded that thermal non equilibrium is more prominent during melting process of PCM in high conductive metal foams and that metal foams can significantly reduce the thermal resistance offered by the PCM. Jin et al. [24], experimentally, investigated the melting of PCM at pore scale level in a metal foam through visualization and concluded that, a smaller pore size improves the melting rate significantly and reduces the thermal non equilibrium between the metal foam and the PCM. Rehman et al. [25] summarized the literature on heat transfer enhancement in PCMs with metal foams. The authors summary states that, metal foams help in uniform temperature distribution in composite PCMs and accelerate the melting process of PCM through their conducting paths. Furthermore, low porosity, high PPI density foams were found to show superior performance in augmenting the heat transfer in metal foam composite PCMs. Abishek et al. [26], numerically, investigated the melting process of composite metal foam PCM at pore scale level by varying the parameters namely strut diameter, pore and cell sizes and specific surface area. The studies reveal that, the metal foam significantly improves the melting rates of PCM and specific surface area of the has a strong correlation with the melting rate of PCM and becomes a vital parameter to optimize the performance of metal foam composite PCM as application specific. Tauseef and Hafiz [27] experimentally investigated the thermal performance of a composite PCM metal foam heat sink with copper and iron-nickel metal foams filled with RT-35 HC as PCM. The results showed that, copper metal foam reduces the base temperature by 5-6 ^{o}C compared to iron-nickel metal foams. Further, the results revealed that a copper metal foam enhances thermal conductivity by 35 times over a pure PCM and a metal foam with lower porosity shows superior performance over metal foam with more porosity in the charging cycle.

From the above review of literature, it is seen that metal foams improve the melting rates of PCM by diffusing heat through high conductivity metal foam ribs. In literature, the melting process of PCM has been investigated with visualization studies and the effect of different parameters such as porosity, PPI and the effect of foam filling height has also been studied numerically and experimentally. These studies have also concluded that lower porosity and higher PPI show more enhancement in heat transfer in a composite metal foam PCM. Based on numerical simulations, a few studies have proposed a new enhancement technique with linearly varying porosity of metal foam along the height (thereby creating a porosity gradient). However, studies on composite metal foam PCM with porosity gradient lack experimental evidence and detailed comparisons with different arrangements of metal foams. The thermal performance of a composite metal foam PCM heat sink depends on mainly two factors (i) volume of PCM and (ii) effective thermal conductivity. The increase in porosity of metal foam increases the volume of PCM but reduces the effective thermal conductivity. The

parameter PPI density affects the convection in the liquid PCM. The convection in liquid PCM is suppressed more with an increase in the PPI density and it is accelerated with decrease in PPI density. In a heat sink, the heat flows from the bottom to the top (in bottom heating case) and the development of temperature gradients along the height of the heat sink is clearly intuitive. Hence, there is a necessity to engineer the distribution of porosity and PPI density of metal foams to increase the overall thermal performance of the heat sink as the melting rate of PCM is highly dependent on the porosity and PPI of the metal foam.

In this work, experimental investigations are performed to study the thermal performance of a composite metal foam PCM heat sink of different configurations with uniform and non uniform porosity (porosity gradient) of metal foams having fixed PPI density. The melting dynamics of PCM during charging and discharging cycles are numerically investigated through supporting three-dimensional conjugate heat transfer simulations with the non thermal equilibrium model and the enthalpy porosity formulation. Further, the thermal performance of a composite metal foam PCM heat sink with uniform and non uniform PPI density (PPI gradient) of a metal foam having fixed porosity is also studied through numerical simulations. The thermal performance of the heat sink configurations are studied in both the charging and discharging cycles and are quantified for different power levels.

2. Experimental setup

The experimental setup consists of a data acquisition system, a DC power source, a computer and a heat sink assembly. Fig. 1a shows a schematic of the experimental setup used in this study. A heat sink made up of aluminium (6101) and PCM cavity of 38 mm in diameter, 55 mm in height and wall thickness of 5 mm is used in this study. An organic material, n-Eicosane ($C_{20}H_{42}$) which has a melting temperature range of 35 - 42 ^{o}C is used as the PCM [5]. Table 1 shows the thermophysical properties of the materials used in this study. The effect of porosity is studied for aluminium metal foams with a fixed PPI density of 20. Tomography is carried out to characterize the metal foams used in this study [28]. Fig. 1b shows photographs of (a) three dimensional tomography view, (b) sectional view and (c) physical views of the metal foams. The metal foam is cut to the same size of the cavity and is then inserted into the heat sink cavity through tight press fitting method to reduce the contact resistance. The porosity gradients are created through the arrangement of different porosity metal foam slices one over the other. A nichrome wire and mica sandwich heater is attached at the bottom of heat sink to mimic bottom heating condition. The power input given to the electric heater through the DC power source is calculated as

$$P = VI \qquad (1)$$

Where P is power in Watts, V is voltage in Volts and I is current in Amperes. Calibrated K-type thermocouples, five in number (two are at heater and three are on side walls), that are connected to a data acquisition system are used to monitor the transient temperatures of the heat sink. A thick cork insulation is provided at the bottom to reduce the heat loss from the bottom of the heat sink. The top of the heat sink is closed with an acrylic cap, while the heat sink outer surface kept open to ambient.

3. Uncertainty analysis

The uncertainty in the heat input is calculated based on the method of propagation of error. The uncertainties associated with the voltage and the current are taken to be the same as the least count of the device used to measure them (i.e., 0.1 V and 0.01 A
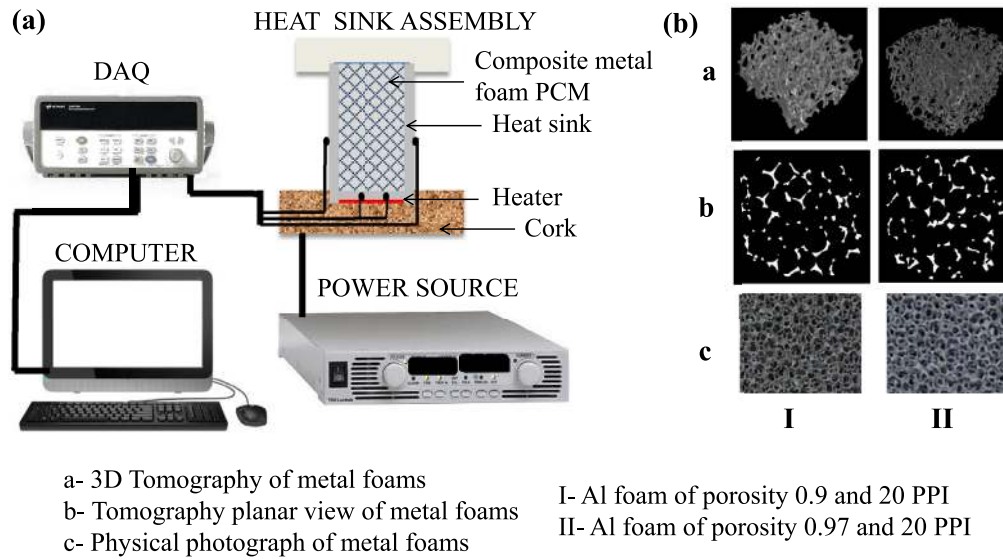
(a) HEAT SINK ASSEMBLY
DAQ
Composite metal foam PCM
Heat sink
Heater
Cork
COMPUTER
POWER SOURCE

(b)
a
b
c
I II

a- 3D Tomography of metal foams
b- Tomography planar view of metal foams
c- Physical photograph of metal foams

I- Al foam of porosity 0.9 and 20 PPI
II- Al foam of porosity 0.97 and 20 PPI

Fig. 1. a) Schematic of the experimental setup. b) Tomography and physical photographs of metal foams.

Table 1
Thermophysical properties of the materials used in this study [36].

Material	$k(\frac{W}{m-K})$	$c_p(\frac{kJ}{kg-K})$	$l(\frac{kJ}{kg})$	$T_m(^oC)$	$\rho(\frac{kg}{m^3})$
n-eicosane	0.39 (solid)	2.1 (solid)	268.2	35 (solidus)	781 (solid)
	0.16 (liquid)	2.42 (liquid)		42 (liquidus)	759 (liquid)
Aluminium	202.4	0.87	-	660.4	2719
Cork	0.045	0.350	-	-	120

for voltage and current respectively). The uncertainty in the heat input is calculated using Eq. (2) as given below

$$\sigma_P = \pm\sqrt{\left(\frac{\partial P}{\partial V}\sigma_V\right)^2 + \left(\frac{\partial P}{\partial I}\sigma_I\right)^2} \quad (2)$$

The uncertainty in the heat input for power level of 10 W is calculated as

$$\sigma_P = \pm\sqrt{(0.73 \times 0.1)^2 + (13.7 \times 0.01)^2} \quad (3)$$

$$\sigma_p = \pm 0.155W \quad (4)$$

$$\frac{\sigma_P}{P} = \pm 0.0155 \quad (5)$$

or ± 1.55%

From the calibration of thermocouples, it is seen that the measurement of temperature has an uncertainty of ± 0.25 °C. One-dimensional heat conduction equation is used to quantify the heat loss from the bottom of heat sink and it is found that there is a maximum of 3% heat loss from the bottom of the heat sink for the given heat input [29].

4. Experimental procedure

In general, to characterize the thermal performance of PCM based heat sinks, two methodologies are widely followed in literature. One is to study the rise of the heat sink temperature till it reaches a set point time, while the other is studying the time till the heater temperature reaches set point temperature. In this work the latter is followed. The charging cycle of heat sink is defined as time interval from the start to the set point temperature when the heat input is given to heat sink. The discharging cycle is defined as the time interval taken from the set point temperature to the ambient temperature, when there is no heat input to the heat sink.

When all the thermocouples show almost the ambient temperature (i.e., 28°C), the heat input is given to the heat sink by the DC power source connected to heater. The charging cycle is studied till the heater temperature reaches the setpoint temperature. After this, the DC power source is switched off to remove the heat input to the heat sink to allow the heat sink to naturally reach the ambient temperature in the discharging cycle. During this complete thermal duty cycle, the transient temperatures are recorded for every 10 s. In this study, experiments have been carried out on the heat sink at ambient temperature of 28 ± 1 ^{o}C for heat inputs of 6, 8 and 10 W. All the experiments are repeated for a significant number of times and the repeatability tests confirmed that the charging and discharging cycles have maximum deviation of less than 3% and 4.2% respectively over the arithmetic mean of repeated runs of experiment. Experimental studies are conducted on a plain PCM heat sink (as baseline) and the studies are extended to different configurations of the heat sink with uniform and non-uniform porosity created with bi-layer metal foams.

5. Numerical modeling

To understand the melting dynamics of PCM three-dimensional numerical simulations have been conducted on the heat sink configurations with metal foams and the numerical results are validated with experimental results. Additionally, numerical simulations are also performed on heat sink with tri-layer metal foams (i.e. porosity gradient created with three layer of metal foams) and average uniform property metal foam (i.e. heat sink with a porosity equal to the mean of the porosities of tri-layer metal foams) to compare the thermal performance of heat sink with bi-layer metal foams (i.e. porosity gradient created with two layer of metal foams). Table 2 shows the list of different metal foam configurations investigated in this present study.

Table 2
Nomenclature of the different configurations investigated in this study.

Heat sink configurations with different porosity gradient metal foams			Heat sink configurations with different PPI density gradient metal foams		
Case	**Study**	**Configuration**	**Case**	**Study**	**Configuration**
Case A-a	Experimental and Numerical		Case B-a	Numerical	
Case A-b	Experimental and Numerical		Case B-b	Numerical	
Case A-c	Numerical		Case B-c	Numerical	
Case A-d	Experimental and Numerical		Case B-d	Numerical	
Case A-e	Experimental and Numerical		Case B-e	Numerical	
Case A-f	Numerical		Case B-f	Numerical	

 Aluminium, Porosity-0.97, PPI-20   Aluminium, Porosity-0.94, PPI-20

 Aluminium, Porosity-0.94, PPI-20   Aluminium, Porosity-0.94, PPI-14

 Aluminium, Porosity-0.9, PPI-20   Aluminium, Porosity-0.94, PPI-8

The enthalpy porosity formulation is used to simulate the phase change process in the PCM and non-thermal equilibrium model is used to simulate the heat transfer process in the porous medium [30]. The governing equations are

The continuity equation:

$$\frac{\partial \rho}{\partial t} + \rho(\nabla \cdot U) = 0 \tag{6}$$

Momentum equation:

$$\frac{\rho}{\varepsilon}\frac{\partial u}{\partial t} + \frac{\rho}{\varepsilon^2}\left(\frac{\partial(uu)}{\partial x} + \frac{\partial(uv)}{\partial y} + \frac{\partial(uw)}{\partial z}\right)$$
$$= -\frac{\partial p}{\partial x} + \frac{\mu}{\varepsilon}\nabla^2 u - \left(\frac{\mu}{K} + \frac{\rho C}{K^{1/2}}|u|\right)u - \frac{(1-\beta)^2}{\beta^3 + \delta}Zu \tag{7}$$

$$\frac{\rho}{\varepsilon}\frac{\partial v}{\partial t} + \frac{\rho}{\varepsilon^2}\left(\frac{\partial(vu)}{\partial x} + \frac{\partial(vv)}{\partial y} + \frac{\partial(vw)}{\partial z}\right)$$
$$= -\frac{\partial p}{\partial y} + \frac{\mu}{\varepsilon}\nabla^2 v - \left(\frac{\mu}{K} + \frac{\rho C}{K^{1/2}}|v|\right)v$$
$$- \frac{(1-\beta)^2}{\beta^3 + \delta}Zv + \rho g\alpha(T - T_l) \tag{8}$$

$$\frac{\rho}{\varepsilon}\frac{\partial w}{\partial t} + \frac{\rho}{\varepsilon^2}\left(\frac{\partial(wu)}{\partial x} + \frac{\partial(wv)}{\partial y} + \frac{\partial(ww)}{\partial z}\right)$$
$$= -\frac{\partial p}{\partial z} + \frac{\mu}{\varepsilon}\nabla^2 w - \left(\frac{\mu}{K} + \frac{\rho C}{K^{1/2}}|w|\right)w - \frac{(1-\beta)^2}{\beta^3 + \delta}Zw \tag{9}$$

Energy equations:

For PCM:

$$\varepsilon\rho\left(c_p + l\frac{d\beta}{dT}\right)\frac{\partial T}{\partial t} + \rho c_p\left(u\frac{\partial T}{\partial x} + v\frac{\partial T}{\partial y} + w\frac{\partial T}{\partial z}\right)$$
$$= k_{eff}\nabla^2 T + ha(T_{mf} - T) \tag{10}$$

For metal foam:

$$(1-\varepsilon)\rho c_p\frac{\partial T_{mf}}{\partial t} = k\nabla^2 T_{mf} - ha(T_{mf} - T) \tag{11}$$

Energy equation for the solid:

$$(1-\varepsilon)\rho c_p\frac{\partial T}{\partial t} = \nabla \cdot k\nabla T \tag{12}$$

The liquid fraction of the PCM (β) (Eq. (7)) is 0 when the PCM is in its solid form and it is 1 when the PCM is in its liquid form and in the mushy region the liquid fraction lies between 0 and 1. The liquid fraction is calculated as

$$\beta = 0 \qquad if \quad T < T_s$$
$$\beta = 1 \qquad if \quad T > T_l$$
$$\beta = \frac{T - T_s}{T_l - T_s} \qquad if \quad T_s < T < T_l$$

The heat transfer in the solid heat sink cavity is governed by heat conduction with the bottom heat flux boundary condition and convection boundary condition at the wall. In the present study, the effective thermal conductivity of the metal foam is calculated following Boomsma and Poulikakos [31] based on a tetrakaidecahedron cell model. Later Dai et al. [32] corrected the Boomsma and Poulikakos model to predict the effective thermal conductivity more accurately. The pertinent relations are

$$k_{eff} = \frac{1}{\sqrt{2}(R_A + R_B + R_C + R_D)} \tag{13}$$

$$R_A = \frac{4\sigma}{(2e^2 + \pi\sigma(1-e))k_{mf} + (4 - 2e^2 - \pi\sigma(1-e))k_{PCM}} \tag{14}$$

$$R_B = \frac{(e - 2\sigma)^2}{(e - 2\sigma)e^2 k_{mf} + (2e - 4\sigma - (e - 2\sigma)e^2)k_{PCM}} \tag{15}$$

$$R_C = \frac{(\sqrt{2} - 2e)^2}{2\pi\sigma^2(1 - 2\sqrt{2}e)k_{mf} + 2(\sqrt{2} - 2e - \pi\sigma^2(1 - 2\sqrt{2}e))k_{PCM}} \tag{16}$$

$$R_D = \frac{2e}{e^2 k_{mf} + (4 - e^2)k_{PCM}} \tag{17}$$

Where $\sigma = \sqrt{\dfrac{\sqrt{2(2 - (5/8)e^3\sqrt{2} - 2\varepsilon)}}{\pi(3 - 4\sqrt{2}e - e)}}, \quad e = 0.339 \tag{18}$

The permeability (K) and inertial coefficient (C) in Eq. (7) are calculated using Eqs. (19) and (20) respectively [33].

$$K = \frac{\varepsilon^2 d_k^2}{36\chi(\chi - 1)} \tag{19}$$

$$C = \frac{0.00212(1 - \varepsilon)^{-0.132}(d_f/d_p)^{-1.63}}{\sqrt{K}} \tag{20}$$

The interstitial heat transfer coefficient is incorporated into the model through a separate user defined function (UDF) and is calculated base on the simplified model which considers the metal foam ribs as cylinders [34]. Hence, the flow of liquid PCM over the metal foam ribs is treated as flow over a cylinder. The following correlations are used for estimating 'h' depending on the Reynolds number range.

$$h = \begin{cases} 0.76Re^{0.4}Pr^{0.37}k/d_f, & 0 < Re \leqslant 40 \\ 0.52Re^{0.5}Pr^{0.37}k/d_f, & 40 < Re \leqslant 1000 \\ 0.26Re^{0.6}Pr^{0.37}k/d_f, & 1000 < Re \leqslant 20000 \end{cases} \tag{21}$$

The other structural and geometrical properties[30] are calculated using equations given below,

$$\text{Pore diameter, } d_p = \frac{22.4 \times 10^{-3}}{PPI} \tag{22}$$

$$\text{Strut diameter, } d_f = 1.18\sqrt{\frac{1 - \varepsilon}{3\pi}}d_p \tag{23}$$

$$\text{Interfacial surface area, } a = \frac{3\pi d_f}{d_p^2} \tag{24}$$

$$\text{Characteristic length, } d_k = \frac{\chi}{3 - \chi}d_p \tag{25}$$

Tortuosity coefficient, $\chi = 2 + 2\cos\left(\dfrac{4\pi}{3} + \dfrac{1}{3}\cos^{-1}(2\varepsilon - 1)\right)$

$$(26)$$

Eqs. (6) to (12) are solved using Fluent 15.0 [35]. The convergence criteria for the continuity, velocity and energy equations are given as 10^{-5}, 10^{-6} and 10^{-8} respectively. Second Order Implicit Method for Pressure Linked Equations (SIMPLE) algorithm is used for pressure velocity coupling and the mushy zone constant is taken as 10^7. Initial numerical simulations have been conducted on a three-dimensional model with 65982 grid elements. Further simulations were conducted on different grid sizes with different number of grid elements till the difference in heater temperature is less than 0.05 ^oC for two consecutive grid sizes. The heater temperature of the heat sink (case A-d) at 3200 s for a heat input of 6 W is taken as the parameter to perform the grid independence study. For the grid elements of 65982, 92856, 135754 and 152687, the heater temperature at 3200 s is found to be 42.54, 42.42, 42.38 and 42.37 ^oC respectively. Since, the difference in heater temperature for 92856 and 135724 elements is only 0.04 ^oC, further simulations are carried out on a model with 92856 grid elements. A time step independence study was also conducted and it was found that a time step of 0.1 s gives satisfactory convergence and accuracy of the solution.

5.1. Validation

Initial numerical simulations are performed to validate the experimental results available in literature. For validation, the case of a copper metal foam with 0.9 porosity and 40 PPI density with geometry 10 × 10 × 4.5 cm is chosen among the cases experimentally investigated by Li et al. [13] for a heat input of 4000 W/m^2. Fig. 2 shows the results of Li et al. [13] and numerically obtained (present study) temperature time histories of the composite PCM metal foam heat sink. From the figure it is seen that, the numerical model shows good agreement with experimental results of Li et al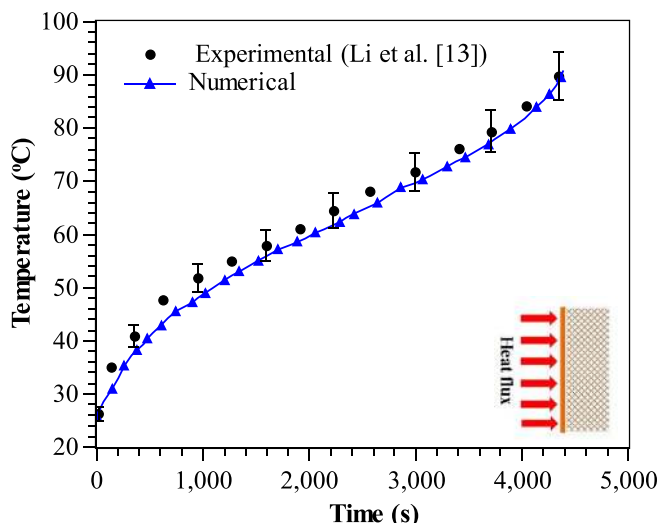. [13] with less than 3% error. Hence, this serves as the independent validation of the numerical model used in the present study.

6. Results and discussion

This section presents results for the charging and discharging cycles for the composite metal foam PCM heat sink. The results are broadly divided into four subsections namely (i) effect of porosity and its gradient, (ii) numerical simulations and melting dynamics of PCM (iii) effect of PPI density and its gradient on the charging cycle and (iv) effect of both porosity and PPI density on the discharging cycle of metal foam composite PCM heat sink. In PCM based heat sinks, the volumetric effect of PCM heat absorption is seen directly in the transient temperature response of the heater. Hence, the transient heater temperature is considered to be the key quantity of interest to evaluate the thermal performance of heat sink. The heat sink with only the PCM (i.e without the metal foam) is taken as the baseline to quantify and compare the thermal performance of different configurations of composite PCM heat sinks with metal foam.

6.1. Effect of metal foam porosity and its gradient on the charging cycle

Fig. 3a-c show the experimentally measured temperature time history of the heat sink heater with different porosity metal foams having constant PPI density of 20 at heat inputs of 6, 8 and 10 W respectively. For a heat sink heated from the bottom, the PCM starts melting from the bottom and side conducting walls. With progress in time, the unmelted solid PCM remains at the center, and due to buoyancy the unmelted solid PCM comes in contact with the bottom. As a result a sudden drop in the heater temperature is seen in the heat sink with PCM case for heat inputs of 6 and 8 W. However, for the case of 10 W due to the rise in temperature caused by self insulation effect of PCM, the unmelted solid PCM does not participate in secondary melting before it reaches the set point temperature [29]. For the cases of heat sink with metal foam, the secondary melting of PCM is not observed as the encapsulation given by the metal foam arrests the movement of solid PCM. For all the heat inputs, it is observed that the heat sink with metal foam shows a higher charging time, regardless of the porosity when compared to a heat sink filled with only PCM. Between the cases of metal foams with uniform porosity, a reduction in the porosity of the metal foam is seen to improve the thermal performance of the charging cycle (i.e., superior performance of case A-b over case A-a) [6]. However, reducing the porosity of metal foam from the bottom to the top (i.e case A-d) shows superiority over both the cases of heat sink with uniform porosity (i.e case A-a and A-b) for the same PPI density of metal foam. A reduction in the porosity increases the metal fraction in the composite metal foam PCM, and this leads to an increase in the effective thermal conductivity. Despite this, the variation in porosity affects the convection in liquid PCM in metal foam (i.e. convection gets suppressed by decreasing the porosity). From the results of this study, it can be inferred that increasing the window of convection in the PCM at the bottom compared to the top enhances the thermal performance of the heat sink. Though case A-e also has non uniform porosity from the bottom to the top (increasing porosity from the bottom to the top) it shows poor performance compared to case A-b despite having the same PPI density. This is speculated as due to reduced convection in the PCM at the bottom due to low porosity and resistance to the heat flow to the top.
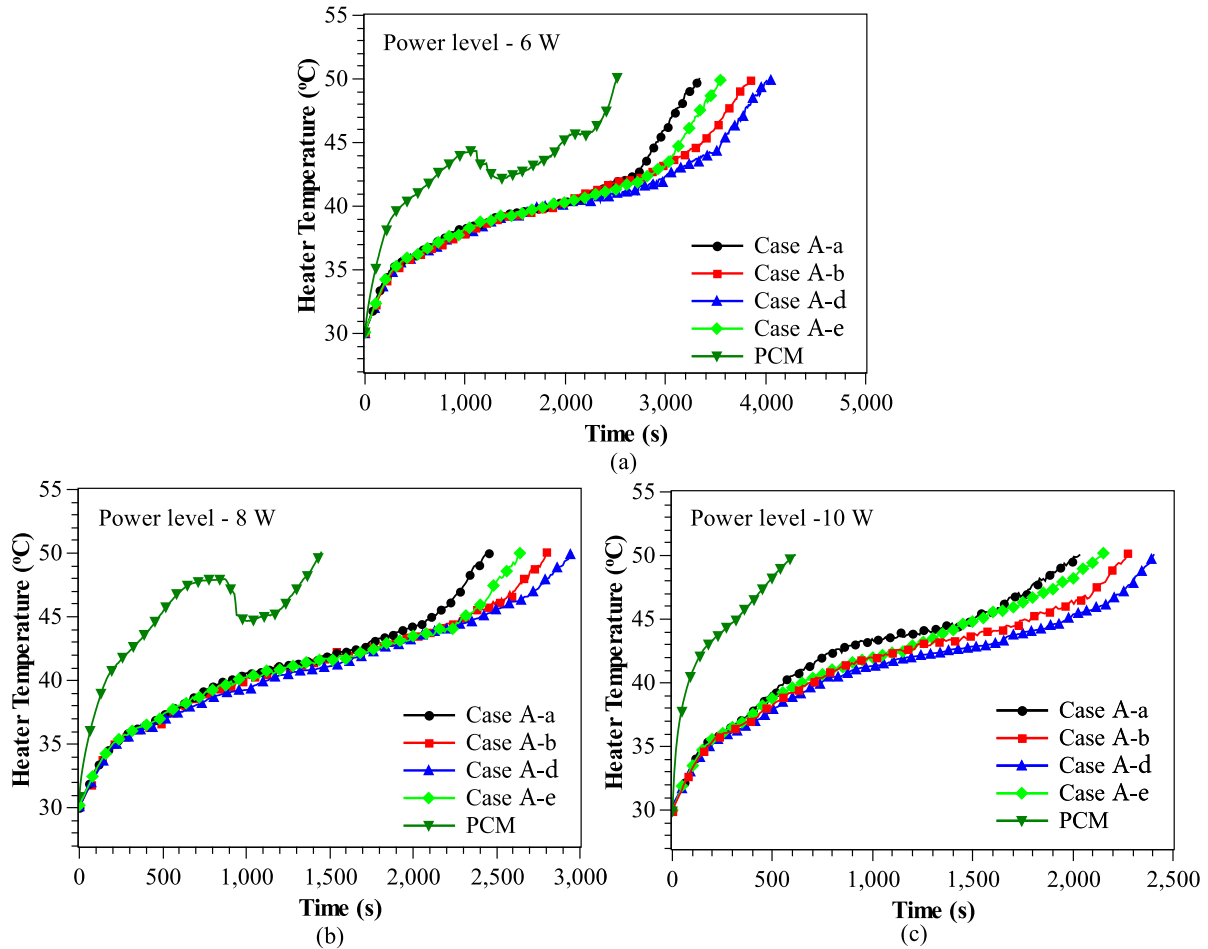

Fig. 2. Validation of the numerical model with the experimental results of Li et al. [13]

Fig. 3. Experimentally obtained transient temperature response of heat sink with PCM and with metal foams in the charging cycle with varying porosity and fixed PPI density for heat inputs of a) 6, b) 8, and c) 10 W.

6.2. Numerical simulations and melting dynamics of PCM in heat sink with metal foams

Fig. 4 shows the experimental and numerical temperature time histories of the heat sink configuration case A-d. From the figure, it is clearly seen that results of the numerical model show good agreement with the experimental results. The temperature time history shows the three energy absorbing regions of the PCM where initial sensible heating of PCM with steep slope (A-B), isothermal phase change with almost constant slope (B-C) an sensible heating of liquid PCM with steep slope (C-D). Time averaged heat transfer coefficients on the surface of heat sink of 12, 9 and 7 W/m^2K showed good agreement with experimental results for heat inputs of 6, 8 and 10 W respectively. These heat transfer coefficients have been applied on the heat sink surface for all configurations and the values for the charging and discharging cycles have been taken to be same for the respective heat inputs. Fig. 5 shows the numerically obtained three-dimensional contours of the PCM liquid fraction during melting at different times. From the figure, it is evident that, the PCM initially starts from the bottom of the heat sink and with progress in time the formation of liquid front takes place at the walls. The simultaneous movement of melt front from the bottom to the top and from the side walls to the center of heat sink cavity completely melts the PCM. Fig. 6 shows the numerical velocity contours of the PCM melting for the heat sink configuration case A-d at different time instances. As seen in the figure, once the PCM starts melting from the bottom there occurs
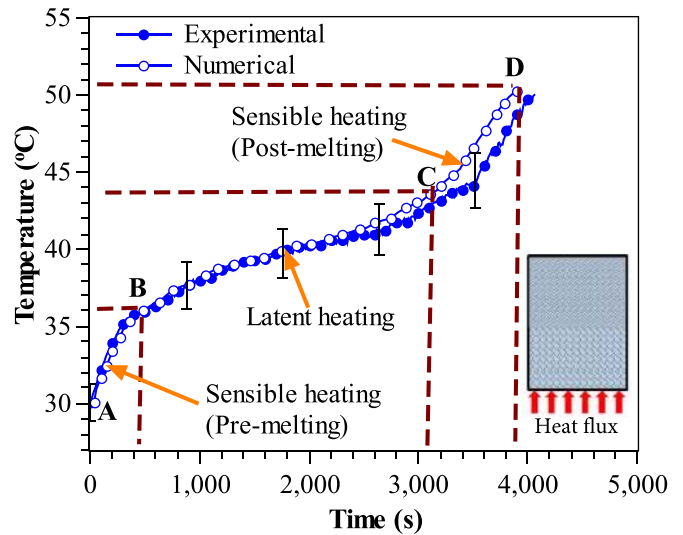

Fig. 4. Validation of the numerical results with in-house experimental results for a heat sink with decreasing porosity from bottom to top (i.e, Case A-d).

formation of two convective velocity cells (~800 s) when a sufficient volume fraction of liquid PCM accumulates at the bottom. As time progresses, the PCM starts melting from the side walls too and these convective velocity cells merge together and form a sin-
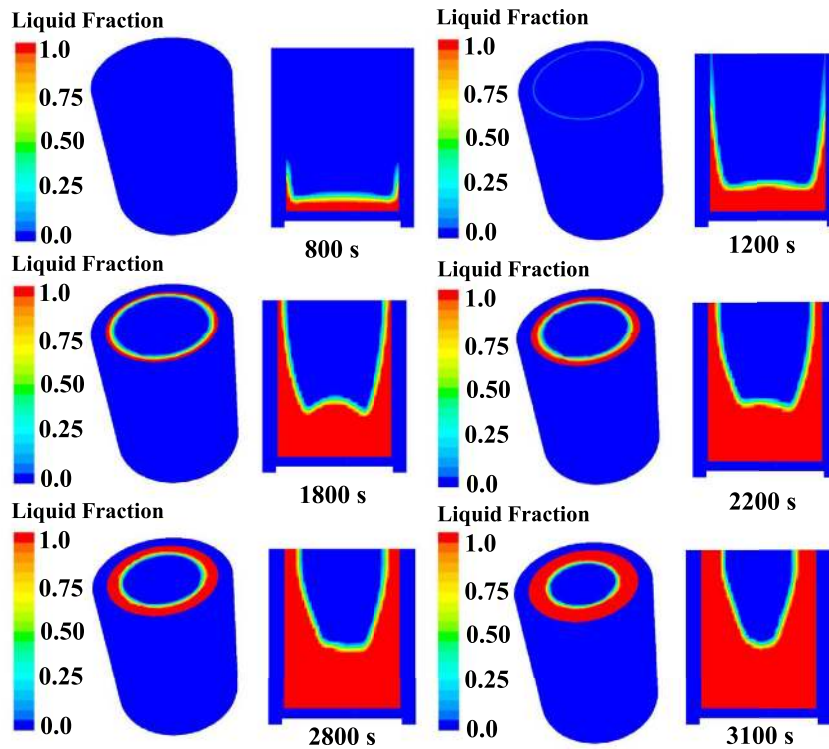
Fig. 5. Numerical liquid fraction contours of the PCM in composite heat sink with decreasing porosity from the bottom to the top (i.e, case A-d) at different time instances for a heat input of 6 W.
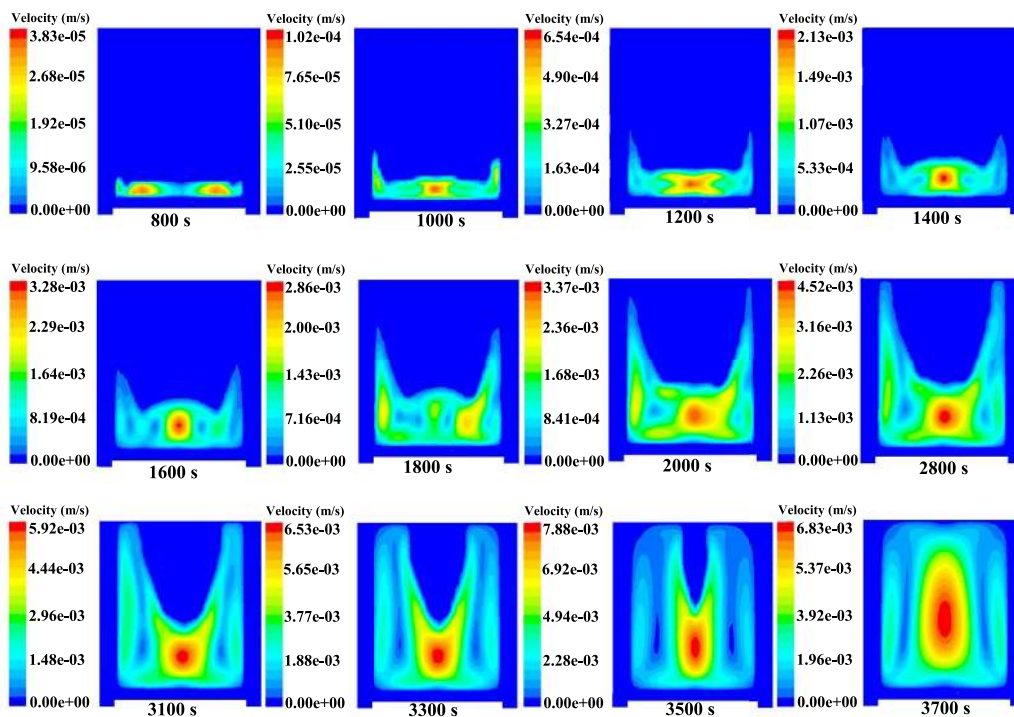

Fig. 6. Numerical velocity contours of the PCM in composite heat sink with decreasing porosity from the bottom to the top (i.e., case A-d) at different time instances.

gle cell (~1000 s) at the center due to presence of liquid PCM near the wall. The cell gradually grows (~1000 to ~1600 s), while the PCM simultaneously starts melting from the side walls too. Once sufficient amount of PCM melts near the wall to create convection cells due to wall temperature in the PCM, cell destruction (~1800 s) and re-formation (~2800 s) with two sub convective velocity cells near the walls take place. Once the convective velocity cells near the side wall form the movement of melt front from the bottom gets suppressed a little and gets accelerated from the side walls at the top of the heat sink (~3100 s to ~3500 s). When the PCM
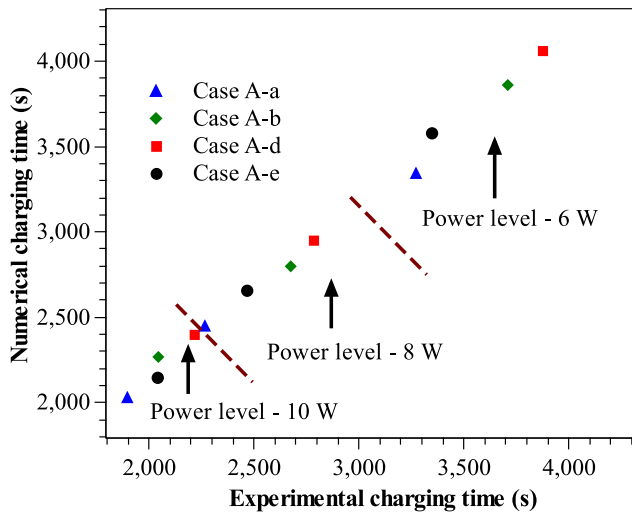
Fig. 7. Comparison of the experimentally and the numerically obtained charging times of the heat sink configurations with uniform and non uniform porosity created with bi-layer metal foams having a fixed PPI density.

completely melts (~3700 s), the center core convective velocity cell grows bigger with two wall sub convective cells and forms three convective velocity cells in the liquid PCM each separated by ve-

locity stratified zones. Numerical simulations are carried out for all the experimentally studied configurations for all heat inputs and similar melting dynamics have been observed. Fig. 7 shows a comparison of the experimentally and numerically obtained charging times for the investigated configurations of heat sink with uniform and non uniform porosity created with bi-layer metal foams having fixed PPI density at different heat inputs. From the figure, it is seen that, for all the heat inputs numerical simulations show good agreement with experimental results in so far as the time to reach set point temperature is concerned, with less than 10% error. This shows the robustness of the model to perform further simulations to carry out (i) further studies on the best performing case of porosity gradient (i.e case A-d) and a tri-layer metal foam (i.e case A-f) and (ii) to compare the thermal performance of uniform porosity metal foam having one porosity which is the mean of porosities of all the metal foams used to create the gradient (i.e case A-c) with the same PPI density.

Fig. 8a-c show the numerically obtained temperature time histories of (i) a heat sink with uniform porosity (i.e case A-c) with porosity value of average of metal foams used to create porosity gradient, (ii) a heat sink with bi-layer porosity gradient (i.e case A-d), and (iii) a heat sink with tri-layer porosity gradient (i.e case A-f) for heat inputs of 6, 8 and 10 W. From the figure, one can observe that the heat sink with porosity gradient (i.e case A-d and A-f) shows superiority in thermal performance over heat sink with uniform porosity metal foam (i.e case A-c) for all the heat inputs.
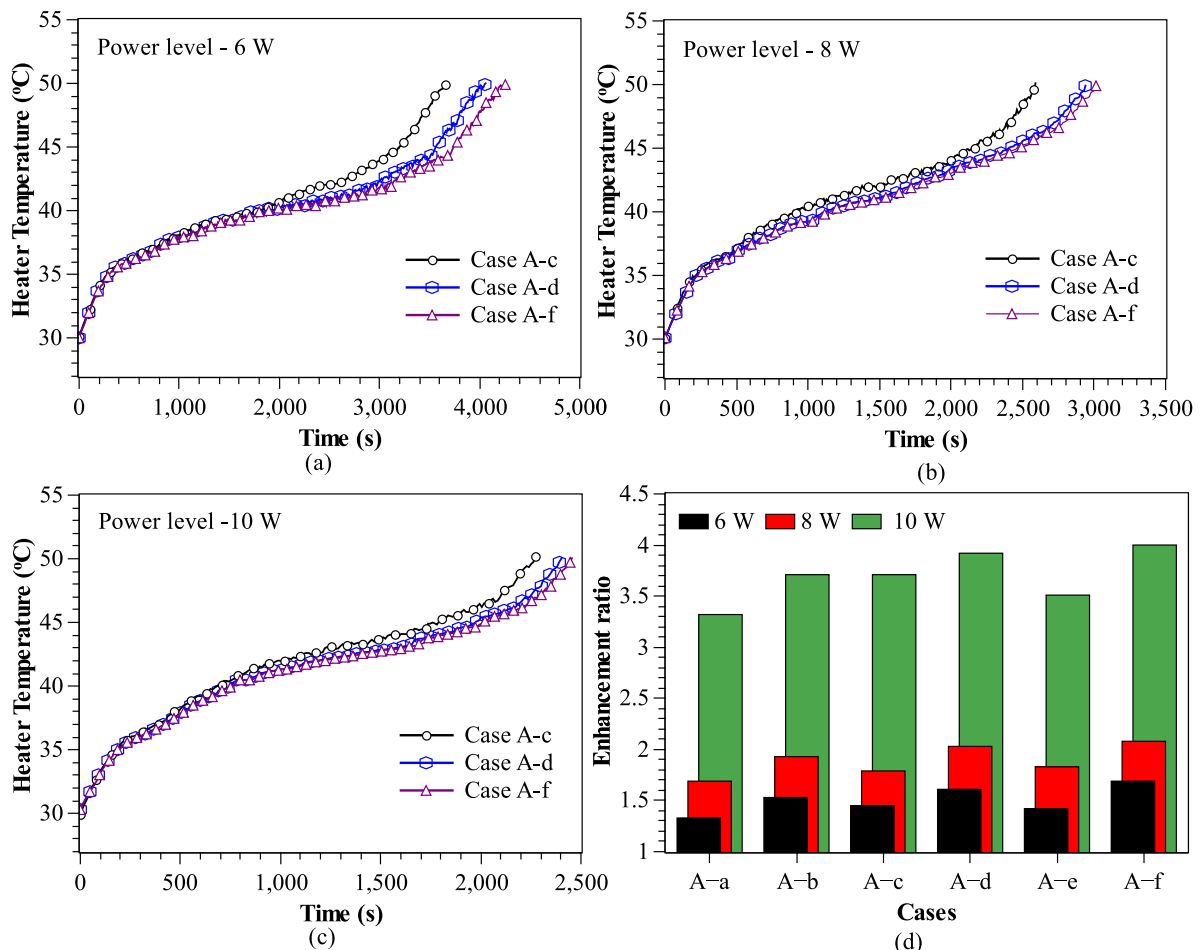

Fig. 8. Numerically obtained temperature time histories of a heat sink with PCM and with metal foams in the charging cycle with varying porosity and fixed PPI density for heat inputs of a) 6, b) 8, c) 10 W and d) Enhancement ratio of the heat sink with different porosities and fixed PPI metal foam configurations for heat inputs of 6, 8 and 10 W based on numerical simulations.

However, heat sink configurations with porosity gradients (i.e case A-d and A-f) shows almost the same performance for all the heat inputs in the charging cycle. This shows that, increasing the linearity in porosity gradient along heat sink height does not improve the thermal performance of the heat sink. This leads to the key engineering conclusion that creating a porosity gradient in a heat sink with two porosity metal foams is good enough for superior thermal performance in comparison with a heat sink with uniform porosity metal foam embedded in it with the same PPI density.

To compare the thermal performance of heat sinks, the charging cycle of heat sink is quantified in terms of non dimensional time which is known as the enhancement ratio and is given as

$$\phi = \frac{t_{mf}}{t_{PCM}} \qquad (27)$$

The quantity, ϕ gives us an idea of the enhancement the metal foam heat sink provides vis-a-vis the plane PCM heat sink in terms of time to reach the set point temperature. Fig. 8d shows the enhancement ratio of heat sinks with composite metal foam PCM for different porosities with constant PPI density and different heat inputs. As the heat input increases, the enhancement ratio also increases due to better heat diffusion from the metal foam compared to a pure PCM at higher power levels. The cases of heat sink with

uniform porosity show enhancement ratios of 1.32, 1.68 and 3.32 for porosity of 0.97 (i.e case A-a) and 1.5, 1.9 and 3.7 for a porosity of 0.9 (i.e case-b) and 1.44, 1.81 and 3.52 for a porosity of 0.94 (i.e case A-c) for heat inputs of 6, 8 and 10 W respectively. The cases of heat sink with non uniform porosity show enhancements of 1.6, 2 and 3.9 for decreasing porosity from the bottom to the top (case A-d) and 1.4, 1.8 and 3.5 for increasing porosity from the bottom to the top (case A-e) and 1.62, 2.15 and 3.9 for decreasing porosity from the bottom to the top in tri-layers (i.e. case A-f) for the same PPI density and heat inputs of 6, 8 and 10 W respectively. All considered, among all the cases of heat sinks with different porosities, the cases of non uniform porosity with reducing porosity from the bottom to the top (i.e case A-d; Bi-layer metal foams and A-f; Tri-layer metal foams) show superiority with enhancements of 21, 19 and 17.4% in the charging time over the composite metal foam PCM heat sink with uniform porosity (case A-a) for 6, 8 and 10 W power levels respectively.

6.3. Effect of metal foam PPI and its gradient on the charging cycle

Fig. 9a-c show the numerically obtained transient heater temperature of PCM metal foam heat sink with varying PPI with fixed
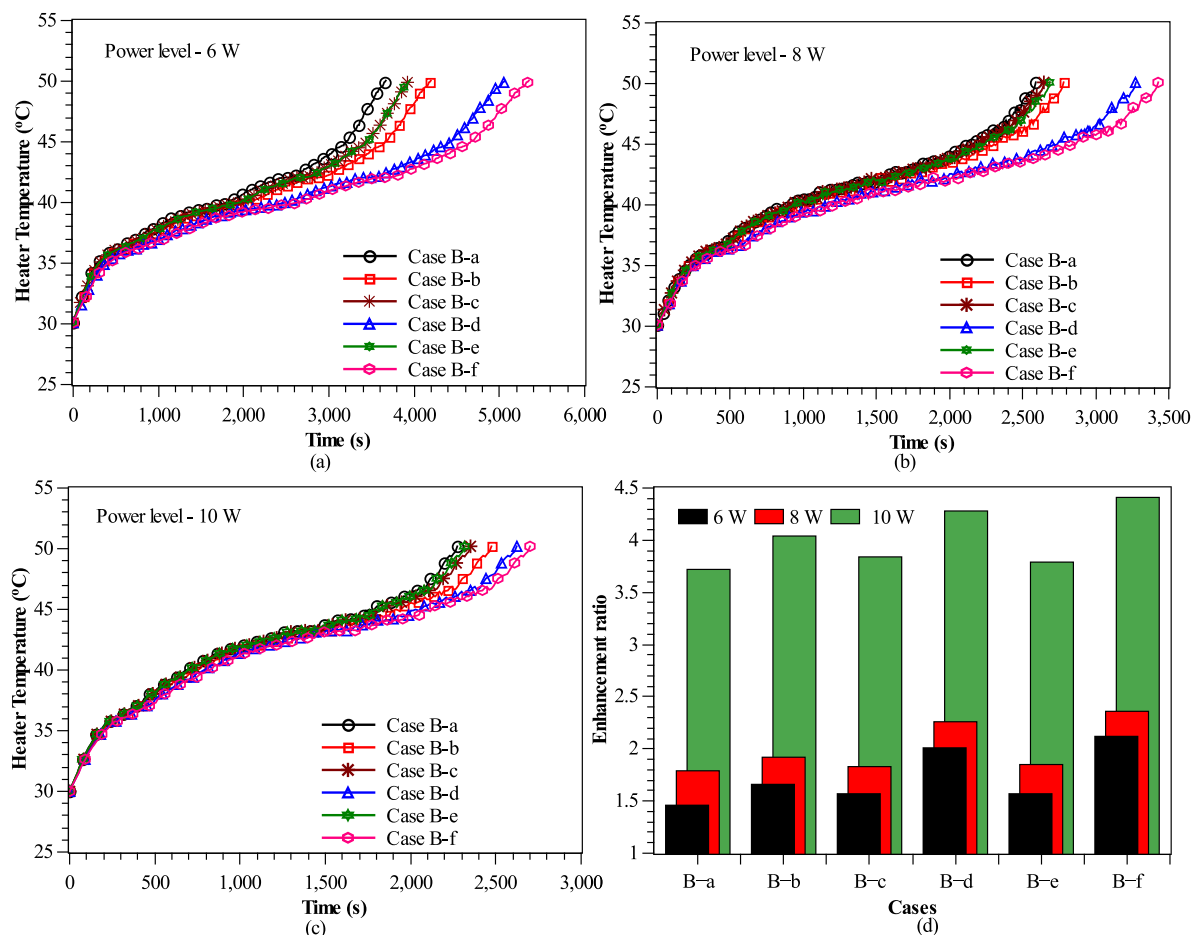

Fig. 9. Numerically obtained temperature time history of a heat sink with PCM and with metal foams in the charging cycle with varying PPI density and constant porosity for heat inputs of a) 6, b) 8, c) 10 W and d) Enhancement ratio of a PCM metal foam composite heat sink for different PPI density and its gradient configurations for heat inputs of 6, 8 and 10 W.

porosity of 0.94 for heat inputs of 6, 8 and 10 W respectively. For all the heat inputs, PCM heat sinks with metal foams maintain the heat source temperatures below the set point for longer periods of time. This reiterates the fact that the metal foam inhibits the convection in the PCM and improves the volumetric energy absorption rate of PCM [8]. Additionally, the metal foam encapsulates the PCM in its pores and accelerates the conduction assisted melting by damping the buoyancy movement of solid PCM. For all the heat inputs, increasing the PPI density seems to enhance the charging cycle of heat sink with uniform foam properties (i.e superior performance of case B-b over case B-a and B-c). However, the heat sink configurations with non uniform PPI (i.e increasing PPI from the bottom to the top cases B-d and B-f) dominate all the configurations with more charging time. This is because of the convection heat transfer in the PCM due to high temperatures at the bottom in the low PPI density metal foam and conduction dominated melting of PCM in the high PPI density metal foam at the top. Though case B-e also has non uniform PPI density (decreasing PPI density from bottom to top), the high PPI density enhances the melting rate of PCM at the bottom due to conduction. The rapid melting of PCM under suppressed convection increases the thermal resistance in this case (i.e case B-e). For all the heat inputs, the heat sink configuration of case B-e shows almost the same performance as that of case B-c. With increase in the heat input the difference in charging time between the uniform PPI density cases(case B-a to B-c) and PPI density gradient cases (case B-d and B-f) gradually reduces. In the charging cycle, among the cases of increasing PPI density from the bottom to the top, the configuration with tri-layer PPI density gradient (Case B-f) shows superiority over the configuration with bi-layer PPI density gradient (Case B-d) in terms of time to reach the setpoint temperature. Fig. 9d shows the enhancement ratio of the PCM heat sink with different foam PPI densities. The figure clearly shows that for all the cases, the enhancement ratio increases with an increase in the heat input. This implies that at higher heat inputs, the metal foams effectively exploit the latent heat of the PCM. The PCM heat sink with metal foam (Case B-a) shows a minimum enhancement of 1.46, 1.79 and 3.72 times over the heat sink with pure PCM for heat inputs of 6, 8 and 10 W respectively. Among the cases of metal foam with different PPI densities, the non uniform PPI density with increasing order PPI from the bottom (i.e case B-f) shows more enhancement with enhancement ratios of 2.12, 2.36 and 4.41 for power levels of 6, 8 and 10 W respectively. These represent a 38, 26 and 19% more enhancement over the heat sink configuration having metal foam with uniform PPI density (Case B-a) for the same heat inputs respectively.

If one considers the charging cycle, between the two parameters porosity and PPI density, the PPI density with its gradient has more effect compared to porosity with its gradient in the thermal performance for the same volume of PCM for all heat inputs.

6.4. Effect of porosity and PPI density of metal foam on the discharging cycle

Fig. 10 shows the experimental and numerically obtained temperature time histories of the PCM metal foam heat sink (Case A-a) in the discharging cycle for a heat input of 6 W. Form the figure, it is evident that, the numerical model shows good agreement with experimental results in the discharging cycle. The energy release stages of the PCM in the discharging cycle are shown where the region EF with steep slope indicates the sensible cooling of PCM (pre-solidification) and latent heat release of PCM in region FG
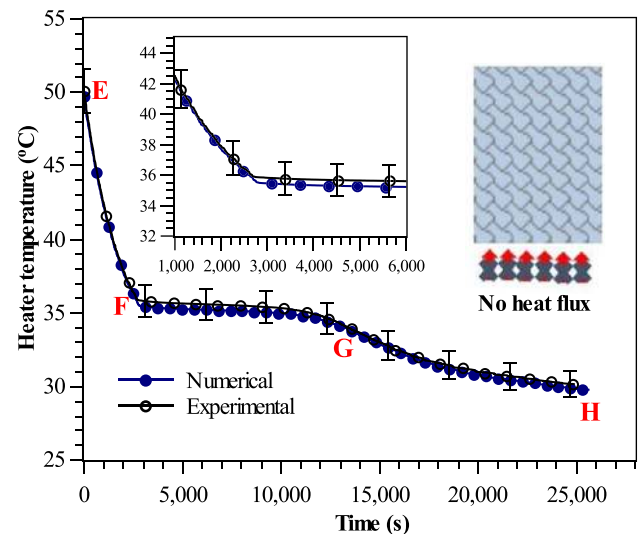

Fig. 10. Experimentally and numerically obtained temperature time histories of a PCM metal foam composite heat sink (Case A-a) in the discharging cycle for heat input of 6 W.

with almost zero slope followed by sensible cooling of PCM (post-solidification) in GH region with a downward slope. Fig. 11a shows the liquid fraction contours of the PCM during solidification of the PCM in the discharging cycle at different instances of time for a typical case (Case A-a) and heat input of 6W. In the discharging cycle, the PCM releases heat through the heat sink walls due to natural convection. From the figure it is seen that, the PCM starts solidifying from the heat sink walls (~2950 s) and this is followed by initiation of the solidification gradually from the bottom (~4000 s). With progress in time, the PCM solidification front simultaneously moves from the bottom and sides and forms a test tube shaped liquid front (~5500 s to ~8500 s). Once the latent heat of the PCM is completely released, the PCM becomes fully solid (after ~10550 s). Fig. 11b shows the velocity contours of the PCM during solidification of PCM in the discharging cycle at different time instances. From the figure, it is seen that during initial stages of solidification three convection cells are seen and their size remain the same due to more liquid fraction of PCM (~2950 s). As the solidification starts from the heat sink walls and the bottom the convection cells near the wall gradually shrink and the center cell moves upward with reducing velocity magnitude (~4000 s to ~5500 s). With decrease in liquid fraction, the convection gets suppressed and the convection cells completely disappear as the solidification process proceeds with velocities approaching zero (~6500 s to ~10550 s). Fig. 12 shows the numerically obtained temperature time histories of the heat sink in the discharging cycle with different porosities (Fig. 12a-c) and PPI densities (Fig. 12d-f) at heat inputs of 6, 8 and 10 W. From Fig. 12a-f, it is seen that, regardless of the porosity and PPI density of the metal foam the heat sink takes almost the same time to reach ambient temperature for all the heat inputs. The PCM heat sink without metal foam is seen to release latent heat with a steep slope unlike a heat sink with metal foam due to non-uniformity in the temperature distribution and poor thermal conductivity compared to the case of PCM heat sink with metal foams. A PCM heat sink without metal foam releases latent heat in the time interval of ~2400 s to ~14000 s for a power level of 6 W, while the PCM heat sink with metal foam releases latent heat between ~2800 to ~11000 s. However, with an increase in the heat input, the heat sink with pure PCM takes almost the same latent
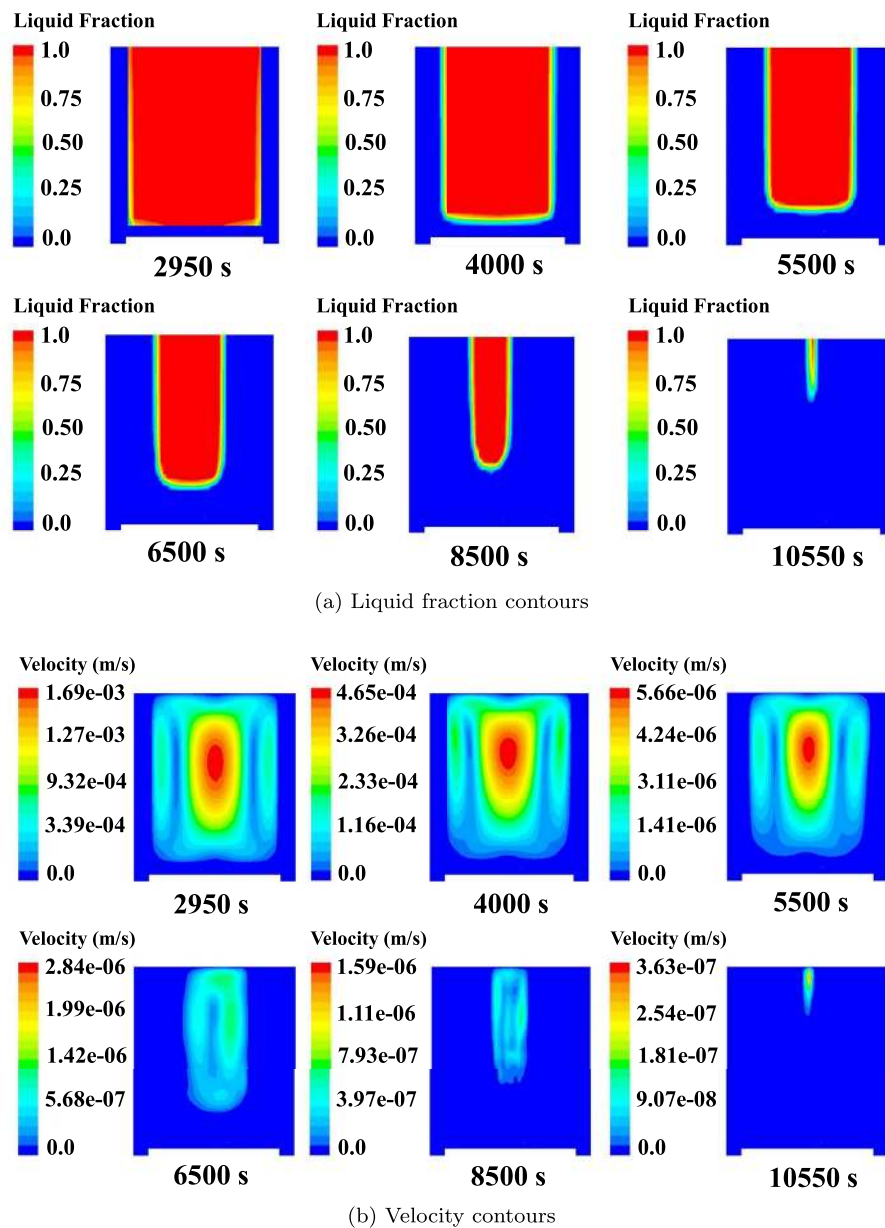
(a) Liquid fraction contours

(b) Velocity contours

Fig. 11. a) Liquid fraction and b) Velocity contours of a PCM composite heat sink (Case A-a) during the discharging cycle at different time instances for heat input of 6 W.

heat release time compared to a heat sink with metal foams due to incomplete exploitation of latent heat during the charging cycle. Regardless of the porosity and PPI density of the metal foam, the composite PCM heat sink takes approximately 14200 s to reach ambient temperature. As there is no heat input at the bottom, all the heat sink configurations start cooling from the same set point temperature with quickly decreasing temperature and velocity gradients which results in low heat transfer coefficient in liquid PCM during the discharging cycle. As the convection is strong in the

heating condition and it gets affected more by the structural and geometrical properties of metal foam, the porosity and PPI exert more influence on the thermal performance of a heat sink in the charging cycle than in the discharging cycle. Further, the outer surface area of the heat sink is fixed irrespective of the composite PCM metal foam configuration in the heat sink and in view of this the porosity and the PPI of metal foam exert only a marginal effect on the discharging cycle of the heat sink.
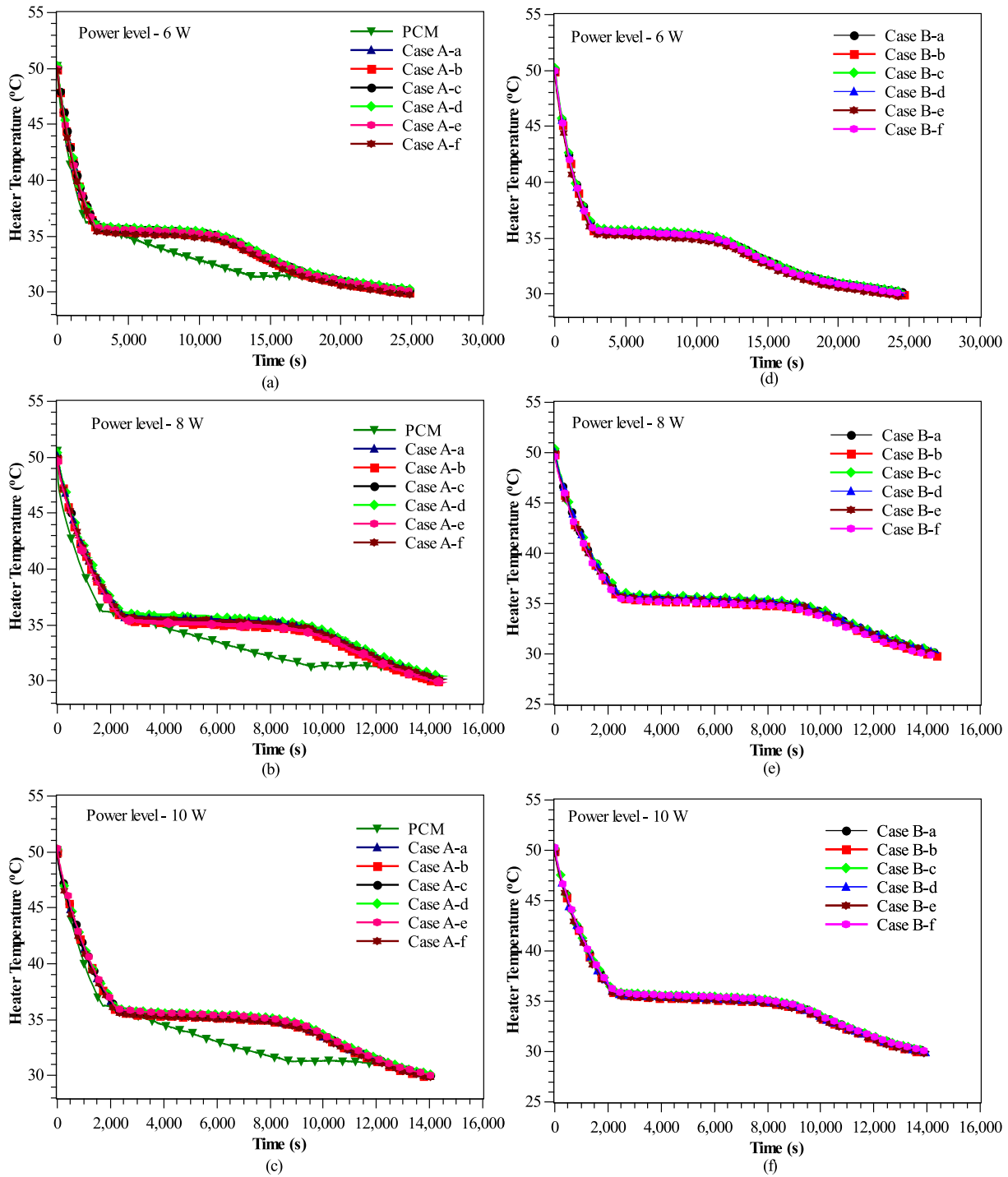
Fig. 12. Discharging cycle of a PCM heat sink without metal foams(experimental) and with metal foams(numerical) with different porosities and its gradients for heat inputs of a) 6 W b) 8 W and c) 10 W and for different PPI densities and its gradients for heat inputs of d) 6 W e) 8 W and f) 10 W.

7. Conclusions

In this paper, the results of experimental and numerical investigations to study the effect of metal foam porosity and its gradient with constant PPI density and the effect of metal foam PPI density and its gradient with constant porosity on the thermal performance of metal foam composite PCM based heat sinks were reported. The phase change dynamics of the PCM in the compos-

ite metal foam heat sink during the charging and the discharging processes were investigated and reported through numerically obtained liquid fraction and velocity contours. From the study it was found that, either decreasing the porosity from the bottom to the top or increasing the PPI density of metal foam from the bottom to the top enhances the thermal performance of the heat sink compared to a heat sink with uniform porosity or uniform PPI density. The salient conclusions from the study are

1. Metal foams enhance the thermal performance of PCM based heat sink upto 4.4 times over a heat sink with pure PCM, in terms of the time to reach the set point temperature.
2. The composite metal foam PCM with non uniform porosity (decreasing porosity from the bottom to the top) enhances the thermal performance of heat sink up to 28% over the heat sink with uniform porosity with the same PPI density in terms of the time to reach set point temperature.
3. The nonuniform PPI density of a metal foam in a composite metal foam PCM shows superiority in thermal performance of heat sink up to 45% over the heat sink with uniform PPI density with the same porosity in terms of the time to reach the set point temperature.
4. The metal foam with PPI density gradient (increasing PPI density from the bottom to the top) for a fixed porosity shows superiority with enhancement ratio of 4.4 among all the composite PCM metal foam heat sink configurations with almost the same volume of PCM, for the charging cycle in terms of time to reach the set point temperature.
5. The porosity of the metal foam and its gradient and PPI density of metal foam and its gradient have very insignificant effect on the discharging performance of the composite metal foam PCM heat sink.

   Between the two parameters porosity and PPI density, engineering the PPI density (increasing from the bottom to the top) in a metal foam in order to use it as a TCE, significantly improves the thermal performance of a PCM heat sink compared to the engineering the porosity of a metal foam. With advanced manufacturing techniques such as 3D printing and additive manufacturing it should be relatively straight forward to create porosity or PPI density gradients in a metal foam to enable its use as a TCE in PCM based heat sinks.

Declaration of Competing Interest

The authors declare no Competing Interest associated with the present work.

Supplementary material

Supplementary material associated with this article can be found, in the online version, at doi:10.1016/j.ijheatmasstransfer.2020.120454.

References

[1] F. Tan, S.C. Fok, Numerical investigation of phase change material-based heat storage unit on cooling of mobile phone, Heat Trans. Eng. 33 (6) (2012) 494–504.
[2] R. Kandasamy, X.-Q. Wang, A.S. Mujumdar, Application of phase change materials in thermal management of electronics, Appl. Thermal Eng. 27 (17-18) (2007) 2822–2832.
[3] S. Mahmoud, A. Tang, C. Toh, A.-D. Raya, S.L. Soo, Experimental investigation of inserts configurations and pcm type on the thermal performance of PCM based heat sinks, Appl. Energy 112 (2013) 1349–1356.
[4] S. Rukh, R.A. Pasha, M.A. Nasir, Heat transfer enhancement of round pin heat sinks using n-eicosane as PCM: an experimental study, Heat Mass Transf. (2018) 1–17.
[5] R. Baby, C. Balaji, Experimental investigations on thermal performance enhancement and effect of orientation on porous matrix filled PCM based heat sink, Int. Commun. Heat Mass Transfer 46 (2013) 27–30.
[6] Z. Qu, W. Li, J. Wang, W. Tao, Passive thermal management using metal foam saturated with phase change material in a heat sink, Int. Commun. Heat Mass Transf. 39 (10) (2012) 1546–1549.
[7] K. Lafdi, O. Mesalhy, S. Shaikh, Experimental study on the influence of foam porosity and pore size on the melting of phase change materials, J. Appl. Phys. 102 (8) (2007) 083549.
[8] Z. Chen, D. Gao, J. Shi, Experimental and numerical study on melting of phase change materials in metal foams at pore scale, Int. J. Heat Mass Transf. 72 (2014) 646–655.
[9] A. Atal, Y. Wang, M. Harsha, S. Sengupta, Effect of porosity of conducting matrix on a phase change energy storage device, Int. J. Heat Mass Transf. 93 (2016) 9–16.
[10] X. Xiao, P. Zhang, M. Li, Effective thermal conductivity of open-cell metal foams impregnated with pure paraffin for latent heat storage, Int. J. Thermal Sci. 81 (2014) 94–105.
[11] H. Zheng, C. Wang, Q. Liu, Z. Tian, X. Fan, Thermal performance of copper foam/paraffin composite phase change material, Energy Conver. Manag. 157 (2018) 372–381.
[12] Y. Tian, C. Zhao, A numerical investigation of heat transfer in phase change materials (pcms) embedded in porous metals, Energy 36 (9) (2011) 5539–5546.
[13] W. Li, Z. Qu, Y. He, W. Tao, Experimental and numerical studies on melting phase change heat transfer in open-cell metallic foams filled with paraffin, Appl. Thermal Eng. 37 (2012) 1–9.
[14] H. Cui, Experimental investigation on the heat charging process by paraffin filled with high porosity copper foam, Appl. Thermal Eng. 39 (2012) 26–28.
[15] S.S. Sundarram, W. Li, The effect of pore size and porosity on thermal management performance of phase change material infiltrated microcellular metal foams, Appl. Thermal Eng. 64 (1-2) (2014) 147–154.
[16] S. Feng, Y. Zhang, M. Shi, T. Wen, T.J. Lu, Unidirectional freezing of phase change materials saturated in open-cell metal foams, Appl. Thermal Eng. 88 (2015) 315–321.
[17] Y. Tao, Y. You, Y. He, Lattice boltzmann simulation on phase change heat transfer in metal foams/paraffin composite phase change material, Appl. Thermal Eng. 93 (2016) 476–485.
[18] F. Zhu, C. Zhang, X. Gong, Numerical analysis and comparison of the thermal performance enhancement methods for metal foam/phase change material composite, Appl. Thermal Eng. 109 (2016) 373–383.
[19] Z. Zhang, X. He, Three-dimensional numerical study on solid-liquid phase change within open-celled aluminum foam with porosity gradient, Appl. Thermal Eng. 113 (2017) 298–308.
[20] Z.-Q. Zhu, Y.-K. Huang, N. Hu, Y. Zeng, L.-W. Fan, Transient performance of a PCM-based heat sink with a partially filled metal foam: Effects of the filling height ratio, Appl. Thermal Eng. 128 (2018) 966–972.
[21] V. Joshi, M.K. Rathod, Thermal transport augmentation in latent heat thermal energy storage system by partially filled metal foam: a novel configuration, J. Energy Storag. 22 (2019) 270–282.
[22] S. Mancin, A. Diani, L. Doretti, K. Hooman, L. Rossetto, Experimental analysis of phase change phenomenon of paraffin waxes embedded in copper foams, Int. J. Thermal Sci. 90 (2015) 79–89.
[23] Y. Yao, H. Wu, Pore-scale simulation of melting process of paraffin with volume change in high porosity open-cell metal foam, Int. J. Thermal Sci. 138 (2019) 322–340.
[24] H.-Q. Jin, L.-W. Fan, M.-J. Liu, Z.-Q. Zhu, Z.-T. Yu, A pore-scale visualized study of melting heat transfer of a paraffin wax saturated in a copper foam: effects of the pore size, Int. J. Heat Mass Transfer 112 (2017) 39–44.
[25] T.-u. Rehman, H.M. Ali, M.M. Janjua, U. Sajjad, W.-M. Yan, A critical review on heat transfer augmentation of phase change materials embedded with porous materials/foams, Int. J. Heat Mass Transf. 135 (2019) 649–673.
[26] S. Abishek, A. King, N. Nadim, B. Mullins, Effect of microstructure on melting in metal-foam/paraffin composite phase change materials, Int. J. Heat Mass Transf. 127 (2018) 135–144.
[27] T.-u. Rehman, H.M. Ali, Experimental study on the thermal behavior of rt-35hc paraffin within copper and iron-nickel open cell foams: Energy storage for thermal management of electronics, Int. J. Heat Mass Transf. 146 (2020) 118852.
[28] A. Elmoutaouakkil, L. Salvo, E. Maire, G. Peix, 2d and 3d characterization of metal foams using x-ray tomography, Adv. Eng. Mater. 4 (10) (2002) 803–807.
[29] G. Kumar Marri, C. Balaji, Experimental and numerical investigations on a phase change material based heat sink with symbiotically joined heat pipe, Heat Transfer Eng. (2019) 1–18.
[30] P. Zhang, Z. Meng, H. Zhu, Y. Wang, S. Peng, Melting heat transfer characteristics of a composite phase change material fabricated by paraffin and metal foam, Appl. Energy 185 (2017) 1971–1983.
[31] K. Boomsma, D. Poulikakos, On the effective thermal conductivity of a three-dimensionally structured fluid-saturated metal foam, Int. J. Heat Mass Transf. 44 (4) (2001) 827–836.
[32] Z. Dai, K. Nawaz, Y. Park, J. Bock, A. Jacobi, Correcting and extending the boomsma–poulikakos effective thermal conductivity model for three-dimensional, fluid-saturated metal foams, Int. Commun. Heat Mass Transf. 37 (6) (2010) 575–580.
[33] J.G. Fourie, J.P. Du Plessis, Pressure drop modelling in cellular metallic foams, Chemic. Eng. Sci. 57 (14) (2002) 2781–2789.
[34] A. Zhukauskas, Heat transfer from a single tubes and banks of tubes in cross-flow, Adv. Heat Transf. 8 (1972) 843–865.
[35] Ansys 15.0 user manual, ANSYS Inc, Canonsburg, PA, USA, 2013.
[36] G.K. Marri, R. Srikanth, C. Balaji, Effect of phase change and ambient temperatures on the thermal performance of a solid-liquid phase change material based heat sinks, J. Energy Storag. 30 (2020) 101327.